JOURNAL OF CATALYSIS 109, 76–88 (1988)

Transmission Electron Microscopy of Ru Supported on Model Oxide Surfaces

A. K. DATYE,*,[1] A. D. LOGAN,* AND N. J. LONG†,[2]

*University of New Mexico, Department of Chemical and Nuclear Engineering, Albuquerque, New Mexico 87131; and †Arizona State University, Center for Solid State Science, Tempe, Arizona 85287

Received February 16, 1987; revised August 18, 1987

The shape and structure of small Ru crystallites have been investigated using transmission electron microscopy (TEM). The Ru crystallites were supported on nonporous submicron oxide particles having simple geometric shapes, e.g., spheres, cubes, etc. The use of such model supports considerably facilitates TEM of small metal crystallites. Since the metal is located on the external surface of the oxide particles, it is possible to observe the crystallites in projection through the oxide as well as edge-on. The profile views yield information on metal–oxide interfaces, contact angles, and wetting. We have found the shapes of Ru crystallites to be similar on both silica and magnesia surfaces. While small crystallites look spherical, the larger crystallites have characteristic ellipsoidal shapes. The larger crystallites are faceted and expose the {00.1}, {10.1}, and {10.0} surfaces of ruthenium.

INTRODUCTION

Transmission electron microscopy (TEM) is a valuable characterization tool for studying heterogeneous catalysts. On a supported metal catalyst, TEM enables the determination of the nature of the dispersed phase (particle size, composition, and habit) and its structural relationship with the support (epitaxial growth, etc.). There is also a great deal of interest in understanding the three-dimensional structure of the metal crystallites and the degree of interfacial interaction (wetting of the oxide, contact angles, etc.). For instance, the phenomenon of strong metal–support interaction (SMSI) has been associated with the metal particles assuming a raft-like or "pill-box" morphology (*1*). In order to study questions such as these, it would be desirable to image the metal crystallites edge-on, with the electron beam parallel to the oxide surface.

However, most high-surface-area catalyst supports have a complex pore structure with the metal crystallites located in the interior as well as on the surface of the pores. Figure 1 shows an electron micrograph of a 2 wt% Ru/MgO catalyst that illustrates some of the problems involved. The majority of the metal crystallites in Fig. 1 are viewed in projection through thin flakes of the oxide support. Thicker regions of the sample generally cannot be imaged well in a TEM due to the loss of resolution by chromatic aberrations and the poor contrast due to multiple and inelastic scattering. The micrograph in Fig. 1 provides no indication of the depth of the metal crystallites normal to the plane of the picture. Attempting to use the contrast of the metal crystallite to infer its three-dimensional shape is misleading as shown by Treacy and Howie (*2*). This is because contrast is dependent on the orientation of the metal crystallites with respect to the electron beam: when oriented correctly for Bragg reflection, a large fraction of the electrons are scattered away and intercepted by the objective aperture causing the

[1] To whom correspondence should be addressed.

[2] Present address: Department of Metallurgy and Science of Materials, University of Oxford, Parks Road, Oxford OX1 3PH, England.

0021-9517/88 $3.00

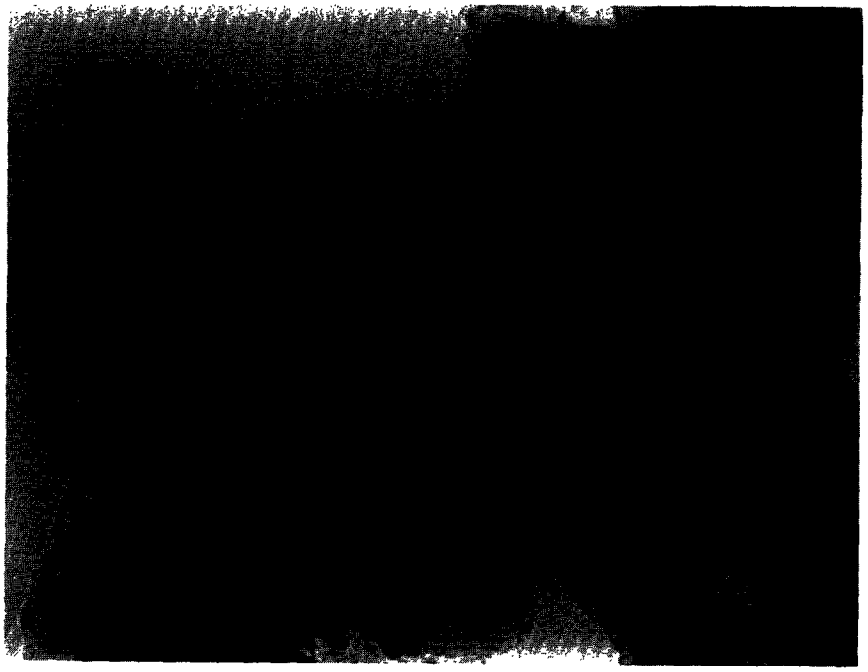

FIG. 1. Electron micrograph of a 2 wt% Ru/MgO catalyst.

metal crystallite to appear dark. If the crystallite is oriented away from a diffracting position, then it appears lighter because only a small fraction of the electrons get scattered away due to inelastic events.

In the literature there is mention of at least two techniques for obtaining the three-dimensional structure of small particles. The topographic contrast technique of Cullis and Maher (*3*) permits pseudo-three-dimensional images to be obtained in a transmission electron microscope. The other technique is weak beam imaging proposed by Yacaman and Ocana (*4*) which enables reconstruction of the three-dimensional structure using the fringe contrast; in practice, the technique is restricted to larger crystallites (>10–15 nm) due to signal intensity limitations. None of these techniques, however, permit an examination of the metal–oxide interface in real space as has been elegantly demonstrated in the area of semiconductor and ceramic interfaces (see Ref. (5) for a review).

To overcome some of the limitations of conventional oxide supports, we have proposed the use of submicron, nonporous oxide particles of simple geometric shape as model supports (*6*). Figure 2 indicates schematically the advantages of such a model support. Since the oxide is nonporous, all the metal is located on the exterior surface. Hence, the sample can be readily tilted to an orientation such that the metal crystallite is imaged edge-on. Further, if the oxide particles are less than a few hundred nanometers in diameter, it is possible to look "through" the oxide and hence image the metal crystallite in projection as well. If

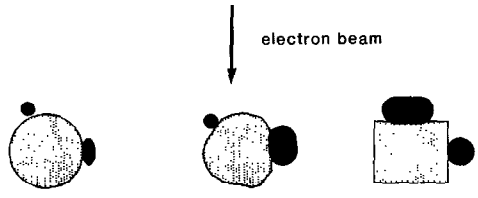

FIG. 2. Schematic diagram illustrating the advantages of simple geometric shapes for studying metal support interactions.

the oxide particles are faceted, it is possible to study the details of the atomic structure of the metal–oxide interface. Furthermore, since the surface area of these oxides is between 10 and 100 m^2/g, it is possible to measure the reactivity of the model catalysts using a conventional flow reactor in a manner comparable to that of conventional supported catalysts.

The use of such model supports opens up the possibility of studying the structure and reactivity of metal crystallites in supported metal catalysts by using the same catalyst for microscopy and reactivity studies. In this paper we discuss the synthesis and characterization of magnesia- and silica-supported model catalysts. Magnesia and silica were chosen for study in view of the differences in the catalytic behavior of Ru supported on these supports. The reactivity of these catalysts will be reported elsewhere (*7*).

EXPERIMENTAL

Catalyst Characterization

Electron microscopy was performed on a JEOL 2000 FX electron microscope operated at 200 keV. In the TEM mode, this microscope has a point resolution of about 0.3 nm. For high-resolution microscopy, a JEOL 4000 EX microscope operated at 400 keV was utilized. With a top entry sample stage, this microscope has a point resolution of 0.17 nm. Catalyst powders were supported on holey carbon film for TEM examination. The ground powder was simply brushed onto the microscope grid to prevent any artifacts or contamination due to the use of solvents. After impregnation and drying, all catalysts were reduced overnight in flowing hydrogen at 400°C. However, the catalysts were exposed to air during sample preparation for microscopy.

Powder surface areas were measured using N_2 adsorption in a Quantachrome Quantasorb analyzer. The samples were outgassed at 110°C for 2 h in flowing helium. A three-point isotherm was fit to the BET equation to determine the total surface area. Metal surface area was determined by static volumetric chemisorption using research purity gases obtained from Matheson. All catalysts had a nominal loading of 2 wt% Ru. Table 1 lists the BET surface areas and H_2 chemisorption uptakes on the catalysts used in this study.

Synthesis of Model Oxide Supports

Model MgO supports were prepared simply by burning magnesium wire in air and collecting the MgO smoke on a solid surface. MgO smoke consists of nearly perfect cubes that expose the {001} surfaces. The {001} surfaces in the rocksalt crystal structure represent an almost abrupt truncation of the bulk structure (*8*). Due to the coordinative unsaturation, there is an "irreversible geometric 'rumpling' of the surface" with oxygen ions rising above the surface plane by 2 pm (*8*). Electron microscopic examination of MgO smoke reveals cubes having flat surfaces and sharp corners. These represent ideal substrates for studying the interaction of the {001} crystal

TABLE 1

Catalysts Investigated

Code	Support	Precursor	BET surface area (m^2/g)	Chemisorption (μmole H_2/g)
RMO3	MgO smoke	$RuCl_3 \cdot 3H_2O$	51.5	16.3
RMO4	MgO smoke	$RuCl_3 \cdot 3H_2O$	6.8	28.9
RMO7	MgO smoke	$Ru(acac)_3$	7.6	12.8
RSO3	130-nm silica spheres	$RuCl_3 \cdot 3H_2O$	23.9	20.3

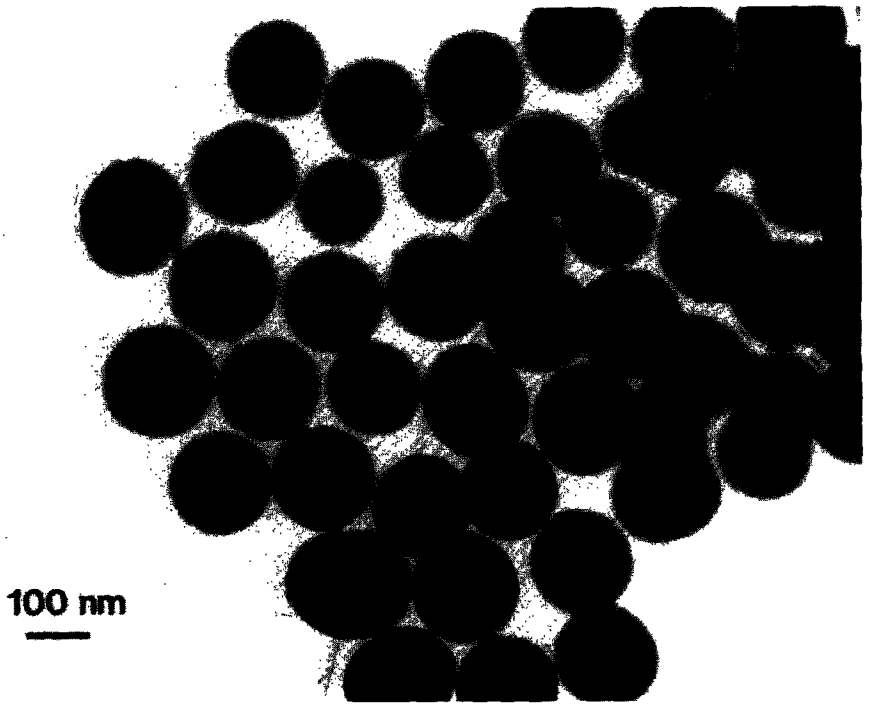

FIG. 3. Micrograph of model SiO_2 spheres (low magnification).

facets with noble metals. MgO cubes prepared by burning Mg wire reveal a broad particle size distribution with the edge length varying between 20 and 500 nm. After preparation, the smoke was stored in tightly capped vials for use in catalyst preparation.

Monodisperse silica spheres were prepared using the technique developed by Strober and Fink (*9*). The reaction involves a hydrolysis of silicon alkoxides in an ethanol solvent using NH_4OH as a catalyst. By varying the reactant concentrations, monodisperse silica spheres having average diameters between 100 and 500 nm can be produced (*10*). These silica spheres are nonporous and have thermal stabilities comparable to commercial silicas. Figure 3 shows an electron micrograph of a batch of 130-nm silica spheres that has been calcined in air at 750°C for 4 h. There is no necking of the silica apparent in this micrograph. A higher magnification view is shown in Fig. 4 where it is seen that the surface of these silica spheres exhibits asperities of the order of 1–2 nm. Silica is mobile under the electron beam and prolonged examination of the silica spheres at high magnifications causes necking of the silica spheres. The spheres break down and lose surface area only after calcination at 1000°C.

RESULTS

Ru/MgO Smoke

Aqueous impregnation was found to be unsuitable for preparing model MgO-supported catalysts due to the readiness with which MgO reacts with water under acidic conditions. While MgO is quite stable to aqueous attack at room temperature in deionized water, the presence of chlorine and the low pH during catalyst preparation using chloride precursors causes complete transformation to the hydroxide phase and

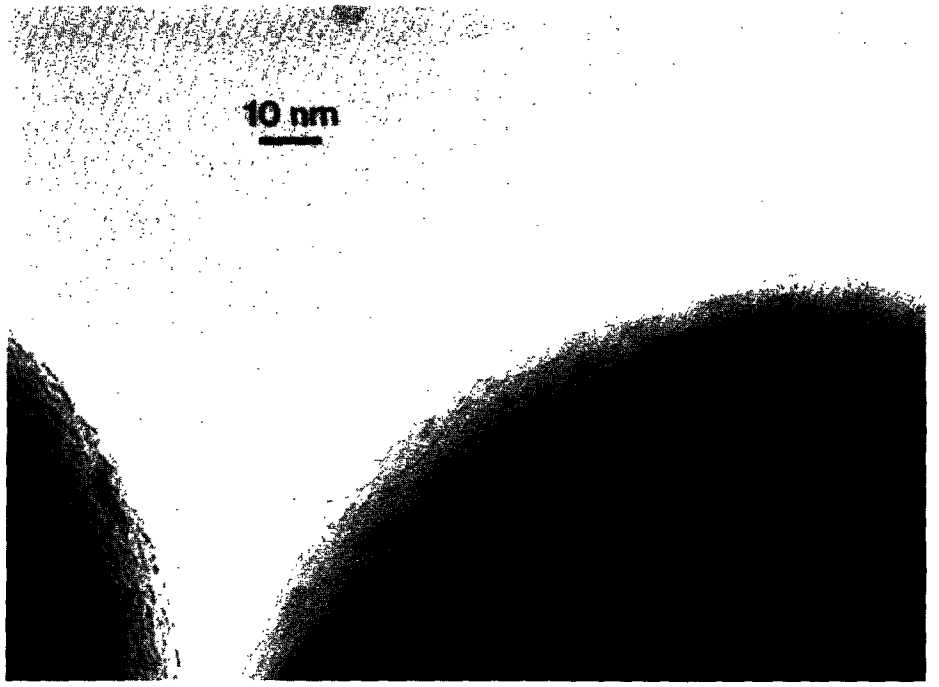

FIG. 4. Micrograph of model SiO_2 spheres (high magnification).

a loss of the cubic morphology (*11*). Figure 5 shows a micrograph of a 2 wt% Ru/MgO catalyst prepared under aqueous conditions using $RuCl_3 \cdot 3H_2O$ as the precursor. The MgO cubes are completely destroyed with the Ru precipitating in the MgO debris surrounding the cubes. Hence, all of the MgO-supported catalysts were prepared under nonaqueous conditions using acetonitrile as the solvent. Acetonitrile was chosen because of the excellent solubility of the $RuCl_3 \cdot 3H_2O$ precursor and the ease with which the solvent could be prepared in anhydrous form.

Figure 6 shows a micrograph of a 2 wt% Ru/MgO catalyst prepared under nonaqueous conditions using the chloride precursor. While the cubic morphology is preserved, it is clear that the MgO surfaces are severely etched due to the chlorine and the water of hydration that is still present in the chloride precursor. High-resolution micrographs show the presence of amorphous material on the surfaces of the MgO cubes. In view of these problems, a nonchloride precursor Ru(III)2,4-pentanedionate (commonly referred to as $Ru(acac)_3$) was used instead.

Figure 7 shows an electron micrograph of a 2 wt% Ru/MgO catalyst prepared using $Ru(acac)_3$ as the precursor. The MgO cubes can be seen to retain their cubic morphology and Ru crystallites can be clearly imaged on the flat {100} surfaces of MgO. Interestingly, most crystallites appear to be flattened out on the surface and assume characteristic ellipsoidal shapes. Figure 8 shows another micrograph of this catalyst where the arrowed Ru crystallite is seen to bend around the edge of the cube and conform to the shape of the cube. This contour replication was widely observed in this catalyst sample. Figure 9 shows a high-resolution electron micrograph of a Ru crystallite on the MgO cubes. Both the Ru and MgO lattices are clearly resolved on the 400-keV microscope. Surface facets on the Ru crystallite reveal the existence of

FIG. 5. Catalyst RMO3: 2 wt% Ru/MgO prepared by aqueous impregnation using $RuCl_3 \cdot H_2O$.

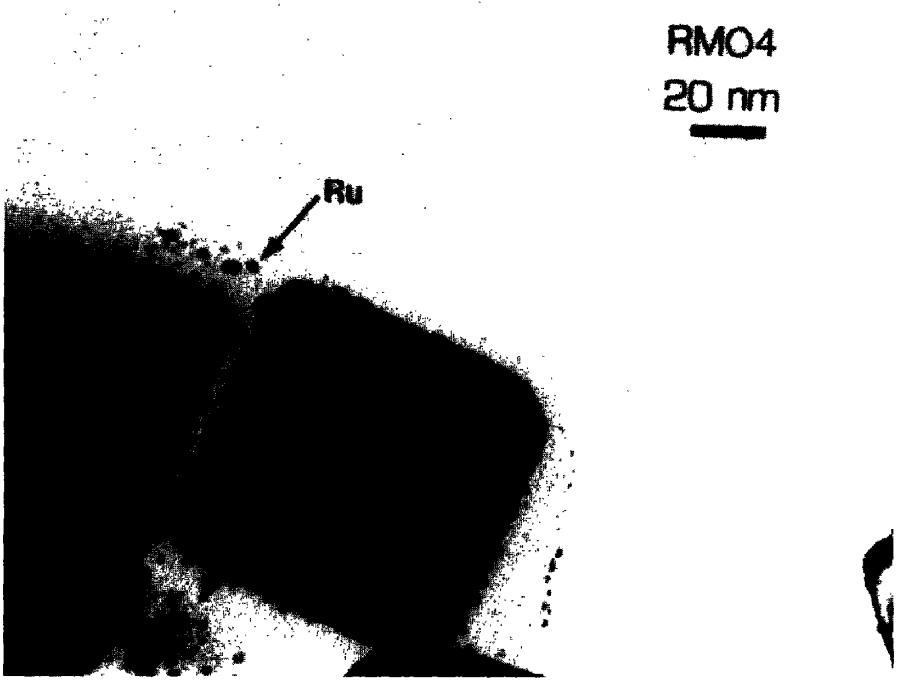

FIG. 6. Catalyst RMO4: 2 wt% Ru/MgO prepared by nonaqueous impregnation using $RuCl_3 \cdot H_2O$.

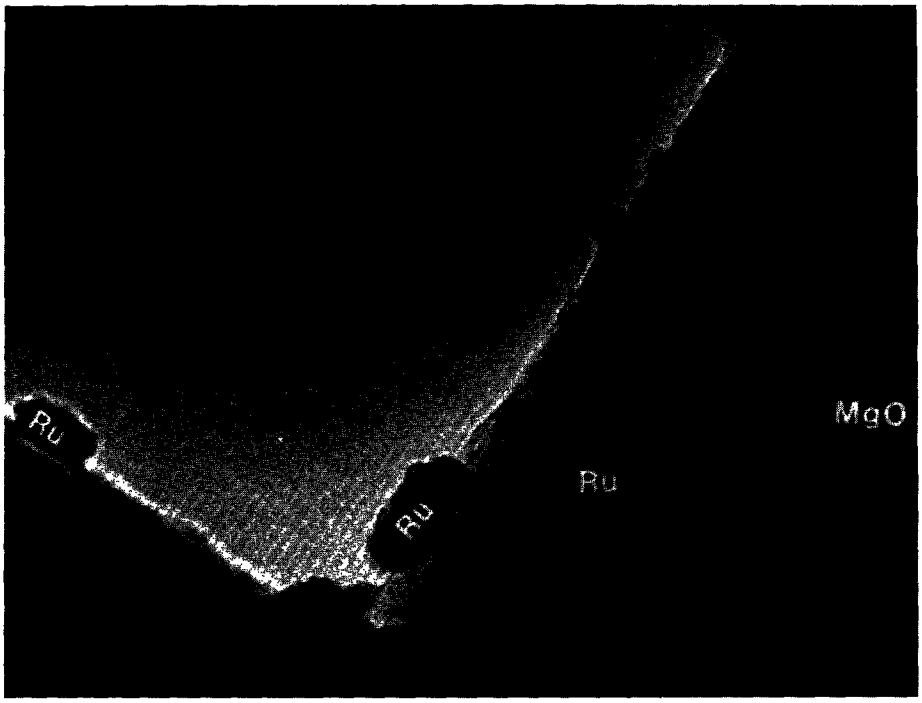

FIG. 7. Catalyst RMO7: 2 wt% Ru/MgO prepared by nonaqueous impregnation using $Ru(acac)_3$. Note the flattened crystallites.

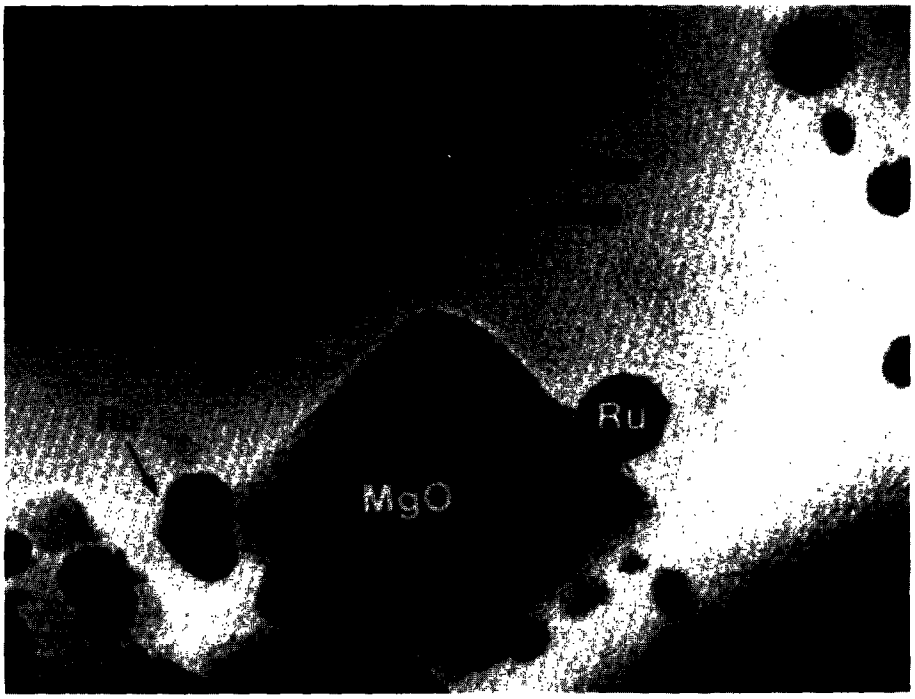

FIG. 8. Micrograph of catalyst RMO7. Note the contour replication.

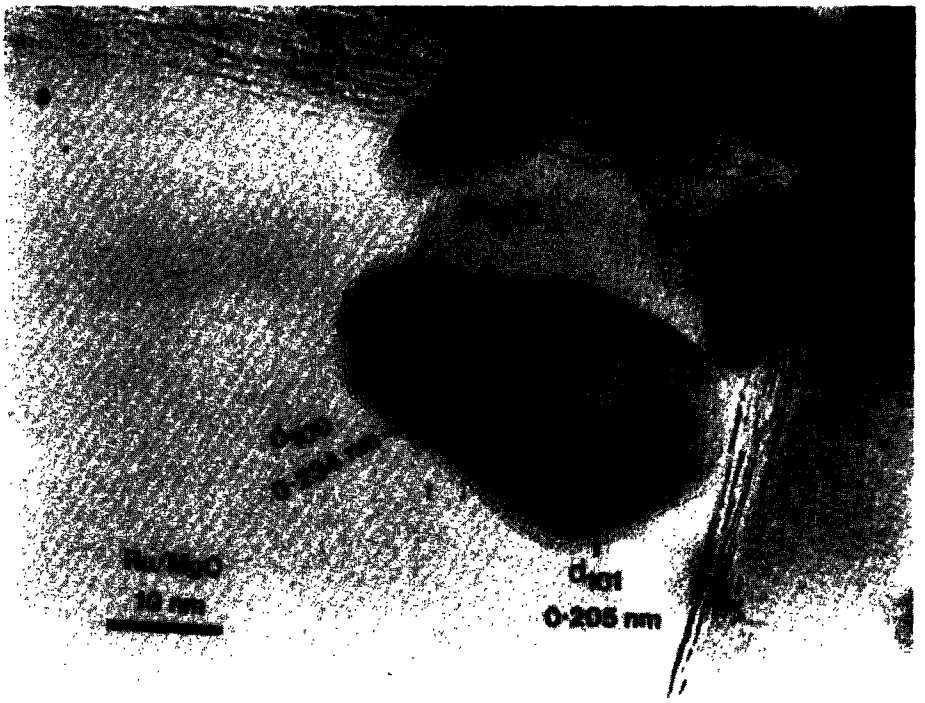

FIG. 9. High-resolution electron micrograph of catalyst RMO7.

preferred low-index planes. An amorphous layer is seen on the surface of the Ru crystallite in Fig. 9. The microscope vacuum was better than 2×10^{-5} Pa; however, the intense electron beam tends to crack any residual hydrocarbon molecules and deposit amorphous carbon. Hence, the surface layer could be amorphous carbon contamination. It is also possible that it represents a surface oxide of Ru formed due to air exposure during sample preparation, or a migration of the support over the metal surface.

The outline of the Ru/MgO interface in Fig. 9 is undulating and rather surprising in view of the known cubic morphology of the MgO support. The undulating profile of the Ru crystallite is caused by the metal bending over the cube edge. This has already been discussed in the context of the lower-resolution micrographs taken on the 200-keV microscope (Fig. 8). The Ru crystallite imaged in Fig. 9 is oriented with the electron beam parallel to the $[1\bar{2}1\bar{3}]$ direction in the hexagonal Ru lattice. Closer examination of the Ru lattice image in Fig. 9 shows a curious fringe pattern in the region close to the MgO surface. This is a moiré effect caused by interference between the Ru and MgO lattice fringes because the Ru/MgO interface is not parallel to the direction of the electron beam. The MgO cube is not oriented along its zone axis as evident from the absence of a cross grating fringe pattern in the MgO lattice fringe image. Hence, it is not possible to infer directly the nature of the Ru/MgO interface from this micrograph. The $(3\bar{2}12)$ crystal plane of Ru is parallel to the MgO cube edge, i.e., the [100] direction. The $(3\bar{2}12)$ surface is not a close-packed, smooth surface, and understanding of the bonding between Ru and MgO will have to await a detailed modeling of this interface. Also evident in the micrograph is an almost one-to-one correspondence between the Ru $(10\bar{1}1)$ $d = 0.205$ nm planes and the MgO (200) $d = 0.21$ nm planes.

FIG. 10. Micrograph of catalyst RMO7. Note the abrupt interface between Ru and MgO.

Figure 10 shows another high-resolution micrograph of this catalyst where a Ru crystallite is located at the edge of the MgO cube. In this micrograph, the MgO cube is close to its zone axis as evidenced by the cross grating fringe pattern for the (002) MgO lattice fringes. The Ru crystallite sits flat on the MgO surface with its basal plane exposed, Ru (0002)//MgO(002). The interface between Ru and MgO is abrupt without any amorphous transition region. The flat interface between Ru and MgO is similar to that seen in several of the crystallites in Fig. 7 indicating it is a preferred mode of nucleation for Ru/MgO.

Ru/Silica Spheres

Figures 11 and 12 show micrographs of a 2 wt% Ru/SiO_2 catalyst. This catalyst was prepared by aqueous impregnation using the chloride precursor. Under these conditions, the distribution of Ru particle size is quite broad with an average particle diameter of 5 nm. Figure 11 shows that while the smaller particles appear spherical, the larger crystallites adopt a characteristic ellipsoidal morphology analogous to that seen on the MgO-supported catalysts. The ruthenium crystallite in Fig. 11 shows surface facets that are very similar to those seen in Fig. 9. The overall three-dimensional shapes of the Ru crystallites seen in Figs. 9 and 10 is remarkably similar to those seen in Figs. 11 and 12, respectively. Despite the different precursors used in preparing the MgO- and silica-supported catalysts, the particle shapes of Ru are remarkably similar on the two supports.

DISCUSSION

The three-dimensional shape of supported metal crystallites, the nature of the metal–oxide interface, and the degree of wetting by the metal are important parameters for heterogeneous catalysts. A number of investigators have studied these

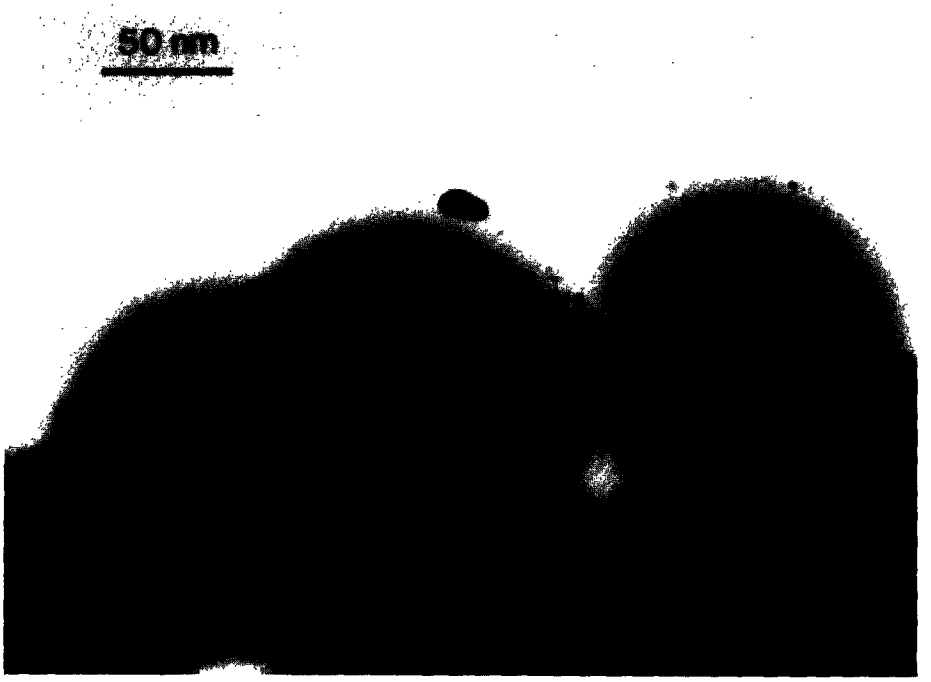

FIG. 11. Catalyst RSO3: 2 wt% Ru supported on 130-nm silica spheres.

parameters by depositing evaporated metal islands on thin support films of oxides or other substrates such as graphite (*12–14*). The shape of the metal crystallites was inferred using indirect techniques such as replication and shadowing. While these indirect methods are quite useful for the study of micron-sized metal crystallites, they are less satisfactory for studying the nanometer-sized crystallites encountered on heterogeneous catalysts. Furthermore, planar oxide supports which are excellent substrates for understanding sintering, redispersion, and surface composition (*15–17*) of supported metal catalysts suffer from the limitation that the metal crystallites are always imaged in projection through the oxide surface. The model supports used in this work offer the possibility of studying metal crystallites in projection as well as edge-on. We have found that a metal loading of 2–5 wt% yields an adequate number of metal crystallites on the oxide surface, obviating the necessity of tilting the sample to obtain profile images.

The electron micrographs of the Ru crystallites on silica and magnesia show that while the small crystallites appear spherical, the larger crystallites appear flattened and assume characteristic ellipsoidal shapes. Many of the larger crystallites show pronounced faceting with the {00.1}, {10.0}, and {10.1} planes of Ru being exposed. The equilibrium shapes of small metal particles in contact with a substrate can be deduced from an extension of the Wulff construction as proposed by Winterbottom (*13*). This analysis would predict the shape to be independent of the size of the particle. The presence of other forces, such as gravity (*18*), can however cause particle shapes to be dependent on size.

It is well known that small droplets of a nonwetting fluid such as mercury on a solid surface are spherical while larger droplets get flattened out due to the influence of

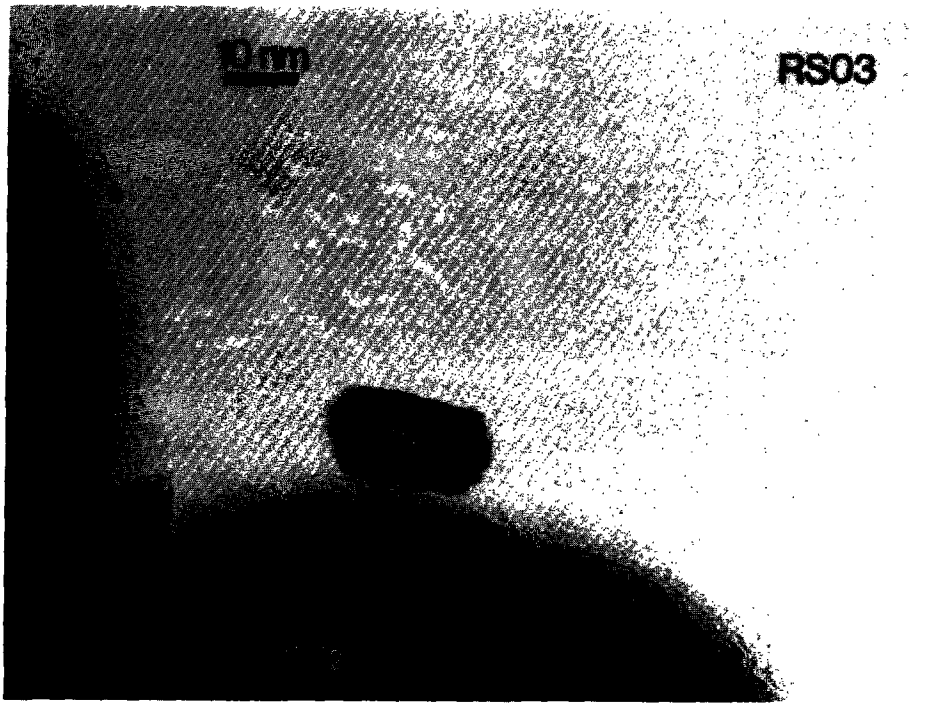

FIG. 12. Electron micrograph of catalyst RSO3.

gravity. While gravity is not expected to affect the shape of the small particles in the supported metal catalyst, the pronounced nonspherical shapes of the large particles may imply the existence of an attractive force between the metal and the oxide that plays a role similar to that played by gravity in the case of sessile liquid drops. The nature of this force is not well understood at this moment and there are indications in the literature that image forces may play a role equal or greater than the expected van der Waals dispersion force (*19*). A variation in particle shape with increased size has also been reported by Anno and Hoshino (*20*). Based on their measurements, they deduced a critical height of 2 nm below which metal particles would be spherical, and above which they would get flattened out. The micrographs in Figs. 3–8 demonstrate that Ru particles considerably larger than 2 nm exhibit spherical shapes. The transition from spherical to flattened shapes must depend on the metal and the specific oxide face in question.

The dependence of the crystallite shape on particle size may also be a consequence of these being nonequilibrium shapes dominated by the kinetics of particle growth. The Ru catalysts used in this work were reduced at 400°C, which is considerably below the melting point for bulk Ru metal (2500°C). In the catalysis literature, considerable importance has been ascribed to the so-called "Tamman temperature = 0.5 T_m" above which small metallic particles are expected to show considerable mobility (*15*). However, the reduction temperature of the catalysts used in this study is less than one-half of the Tamman temperature. Hence, the metal would not be expected to show any liquid-like behavior. Annealing at temperatures close to the melting point will be necessary to determine the equilibrium shapes of these Ru crystallites.

In the MgO-supported catalyst, many of

the crystallites that have nucleated on the corners appear to bend over the edges of the cubes. This contour replication indicates partial wetting of the MgO by the Ru metal. Theoretical analysis of nucleation at steps and kinks (*21*) and corners (*22*) indicates that the contour replication is consistent with partial wetting of the substrate. The contact angle and the overall shape of the Ru crystallites are similar on both the silica and the magnesia supports. The absence of any sharp corners on the silica precluded observation of any contour replication this support.

CONCLUSIONS

The model supports used in this work provide ideal substrates for investigating the shape and structure of small metal crystallites in supported metal catalysts. The model catalysts have BET surface areas comparable to those of conventional supported catalysts such that their reactivity can be measured in a flow reactor using the same catalyst that is used for doing the microscopy. This overcomes the limitations in the use of planar model supports which have low surface areas and require the use of UHV techniques for characterizing reactivity. On oxide supports that have well-defined facets, it is possible to observe the atomic structure of the metal–oxide interface. The edge-on views can help answer questions concerning interfacial contact angles, wetting, and spreading of the metal on the oxide, and hence improve understanding of metal–support interactions. A further advantage is that when the morphology of the model support is known, any changes in the oxide caused by the catalyst impregnation process can be readily identified. In the context of metal–support interactions, Bond (*23*) has classified MgO and silica supports as weakly interacting. This is borne out in our work in view of the similarity in shape of the Ru crystallites on these supports. Other supports, such as TiO_2 and Nb_2O_5 which exhibit SMSI, may have more pronounced effects on the shape and structure of metal crystallites.

ACKNOWLEDGMENTS

We thank Dr. R. K. P. Zia for sending us preprints of his paper and Dr. R. I. Masel for bringing the paper to our attention. This work was supported by a grant from the Engineering Foundation, and from Sandia National Laboratories. Electron microscopy was performed at the electron microbeam analysis facility within the Department of Geology and Institute for Meteoritics at UNM. High-resolution electron microscopy was performed at the Center for solid state science, Arizona State University, which is supported by NSF (Grant DMR-86-11609).

REFERENCES

1. Baker, R. T. K., Prestridge, E. B., and Garten, R. L., *J. Catal.* **56,** 390 (1979).
2. Treacy, M. M. J., and Howie, A., *J. Catal.* **63,** 265 (1980).
3. Cullis, A. G., and Maher, D. M., *Ultramicroscopy* **1,** 97 (1975).
4. Yacaman, M. J., and Ocana, Z., *Phys. Stat. Sol.* **42,** 571 (1977).
5. Krivanek, O. L. (Ed.), "Atomic Scale Structure and Properties of Interfaces." Proc. of a workshop held at Wickenberg, AZ, 1984; published as *Ultramicroscopy* **14** (1984).
6. Datye, A. K., and Logan, A. D., "Proc. 44th Meeting of the Electron Microsc. Soc. Amer." (G. W. Bailey, Ed.), p. 772. San Francisco Press, 1986.
7. Logan, A. D., and Datye, A. K., submitted.
8. Welton-Cook, M. R., and Berndt, W., *J. Phys. C* **15,** 5691 (1982).
9. Strober, W., and Fink, A., *J. Colloid Interface Sci.* **26,** 62 (1968).
10. Huizenga, D. G., and Smith, D. M., *AIChE J.* **32,** 1 (1986).
11. Holt, T. E., Logan, A. D., Chakraborti, A., and Datye, A. K., *Appl. Catal.*, in press.
12. Sundquist, B. E., *Acta Metal.* **12,** 67 (1964).
13. Winterbottom, W. L., *Acta Metal.* **15,** 303 (1967).
14. Pilliar, R. M., and Nutting, J., *Philos. Mag.* **16,** 181 (1967).
15. Ruckenstein, E., *in* "Sintering and Heterogeneous Catalysis" (G. C. Kuczinski, A. E. Miller, and G. A. Sargent, Eds.), Material Science Research, Vol. 16, p. 199. Plenum, New York, 1984.
16. Lee, C., and Schmidt, L. D., *J. Catal.* **101,** 123 (1986).

17. Nakayama, T., Arai, M., and Nishiyama, Y., *J. Catal.* **87,** 108 (1984).
18. Zia, R. K. P., and Gittis, A., *Phys. Rev. B* **35,** 5907 (1987).
19. Stoneham, A. M., and Tasker, P. W., *J. Phys. C* **18,** 543 (1986).
20. Anno, E., and Hoshino, R., *Surf. Sci.* **144,** 567 (1984).
21. Lee, J. K., and Aaronson, H. I., *Surf. Sci.* **47,** 692 (1975).
22. Zia, R. K. P., Avron, J. E., and Taylor, J. E., "The Summertop Construction: Crystals in a Corner," submitted.
23. Bond, G. C., *in* "Metal–Support and Metal–Additive Effects in Catalysis" (B. Imelik *et al.*, Eds.), p. 1. Elsevier, Amsterdam, 1982.